Indian Journal of Engineering & Materials Sciences
Vol. 31, October 2024, pp. 641-649
DOI: 10.56042/ijems.v31i5.10855

Investigation on effect of fly ash based geopolymeric coated BOF steel slag as coarse aggregate in concrete

Pratik Kumar Goyal[a,*], Pradeep Kumar Ghosh[a] & Manish Mudgal[b]

[a]University Teaching Department (UTD), Chhattisgarh Swami Vivekanand Technical University, Bhilai (C.G.) 491 107, India

[b]Centre for Advanced Radiation Shielding and Geopolymeric Materials (CARS & GM),
CSIR-Advanced Materials and Processes Research Institute, Bhopal (M.P.) 462 026, India

Received: 20 May 2024; accepted: 20 September 2024

Considering the notable depletion of natural resources, leveraging basic oxygen furnace (BOF) steel slag (SS) aggregate as a replacement for natural coarse aggregate in concrete presents a promising technological response. The expansive properties of SS, attributed from the existence of free-CaO, present obstacles in achieving efficient utilization of concrete. This study explores the use of fly ash-based geopolymer-coated steel slag aggregate within a geopolymer matrix concrete, focusing on its influence on the compressive performance of the concrete. Three geopolymer pastes with varying molarities of sodium hydroxide (6M, 12.5M, and 16M), each with equal sodium silicate content, have been considered experimental parameters for the complete replacement of natural coarse aggregate. Preliminary examinations has encompassed morphological, mineralogical, and microstructural analyses of fly ash and BOF steel slag, employing techniques such as XRF, SEM, XRD, FT-IR spectroscopy, and Optical microscopy. Furthermore, a series of axial compression tests have been conducted on geopolymer-coated steel slag geopolymer concrete. The findings have revealed that geopolymer paste with higher molarity establishes superior physical bonding between SS and the concrete matrix, exhibiting enhanced inhibition of SS expansion and consequently resulting in superior compressive strength. This research has emphasized the effective utilization of BOF SS coated with fly ash geopolymer as coarse aggregate in an unreinforced concrete product made with a fly ash-based geopolymer binder. This approach reduces waste, improves material handling, and mitigates environmental pollution.

Keywords: Steel slag, Fly ash, Geopolymer concrete, Compressive strength

1 Introduction

The development of any community is often measured by key parameters, with the steel industry playing a crucial role in this evaluation[1].In the context of India's economic progress, the steel industry significantly contributes to its development[2]. According to the World Steel Association report issued on the year 2021[3], the global manufacturing of crude steel amounted to around 1878 million tons (MT). China is at the forefront of total crude steel production, contributing 56.7% with 1064.8 MT, trailed by India, which accounts for 5.3% with 100.3 MT. Globally, roughly 73.2 percent of crude steel manufacturing comes from oxygen route furnaces, while the remainder is generated through electric route furnaces. Whereas, in India, data indicates that 45% of furnaces are of the basic oxygen variety, with the remaining 55% operating under electric arc furnaces. During the molten iron to steel conversion process, slag is produced as a secondary outcome while mixing scrap iron and fluxes like lime/dolomite to eliminate impurities. This slag, a complicated mixture of oxide and silicate that solidifies when cooled[4]. Currently, Slag is disposed away in landfills as garbage[5], occupying significant land areas and causing environmental pollution (soil, water, and air) due to alkali leaching[6-9]. Based on estimation, integrated steel mills generate over half a metric ton of steel slag (SS) per metric ton of steel manufactured[10, 11]. There are four primary types of slag generated during the iron-to-steel conversion process, categorized by the method employed: blast furnace, electric arc furnace, BOF, and ladle furnace slag. Recent studies have explored the usage of BOF SS in road construction aggregate[12-15]. Nevertheless, its application is limited due to volume expansion issues stemming from the presence of free lime and free magnesia. The concentration of free lime in BOF SS can range from 1% to 10%[16, 17]. Therefore, weathering, or ageing, is considered a natural solution to address expansion problems, requiring around 12 months. This process involves exposing the material

*Corresponding author(E-mail: pratik94.g@gmail.com)

to open atmosphere conditions for an extended duration, reducing f-CaO content to less than 2%. The period of ageing may vary based on variables like humidity and the original free lime content[5, 6, 18, 19]. The reduction process is driven by the BOF SS absorbing moisture (H_2O) and carbon dioxide (CO_2) from the atmosphere. This procedure results in the generation of calcium hydroxide by the interaction of free calcium oxide (f-CaO) with moisture, subsequently undergoing a reaction with CO_2 to yield calcium carbonate ($Ca(CO)_3$)[20]. The hydration of free calcium oxide, producing $Ca(OH)_2$, is the primary cause of expansion and disintegration. Over time, as these reactions continuously occur, the overall potential expansion of slag decreases. Despite its time-consuming nature, weathering or ageing proves economically viable. Geopolymer binder (GB) emerges as the third-generation binder in concrete production, succeeding lime and ordinary Portland cement[21].GB can replace traditional cement products by utilizing aluminosilicate solids like fly ash (FA), metakaolin, red mud, and rice husk ash, among others[22-25]. Compared to conventional cementitious binders, GB boasts a significantly reduced carbon footprint[26]. The creation of a geopolymer binder (GB) entails the activation of aluminosilicate source materials using alkali solutions. As a result, geopolymer concrete (GC) emerges as a feasible substitute for traditional concrete, demonstrating superior initial strength and improved resistance to harmful acids[27], reduced permeability, resistance to elevated temperatures[28], increased resilience against freeze and thaw cycles[29], and improved thermal insulation[30].

In this research, the focus is on addressing the expansion issues associated with BOFSS and inhibiting expansion by employing a coating of fly ash geopolymer. The intention is to enhance the properties of geopolymer concrete built with BOF SS, specifically the compressive strength, by substituting this coated slag for natural aggregate as a coarse aggregate. The study involves the use of three different molarities of NaOH (6M, 12.5M, and 16M) along with an equal amount of sodium silicate to formulate the geopolymer coating solution. The investigation encompasses morphological, mineralogical, and microstructural analyses of both fly ash and BOF steel slag, utilizing techniques such as XRF, SEM, XRD, and FT-IR spectroscopy. Additionally, the performance of the developed concrete is assessed through compressive strength tests, and the microstructural analysis is conducted using optical microscopy.

2 Materials and Methods

2.1 Materials

Fly Ash (FA), categorised as class-F in accordance with IS 3812:2013[31] specifications, was sourced from NSPCL, Bhilai (C.G.), INDIA. The specific gravity of FA was 2.1, and it underwent oven drying at 100°C for four hours before utilization. BOF steel slag, also referred to as Linz-Donawitz (LD) slag commonly denoted as Steel Slag (SS), was collected from Bhilai Steel Plant (BSP), Bhilai, India, and employed as coarse aggregate. The SS exhibited a specific gravity of 2.75, along with a water absorption rate of 1.29% and an apparent porosity of 3.07%. Locally available River Sand (RS) was chosen as fine aggregate, adhering to IS 383:2016[32] guidelines for zone II. The RS exhibited specific gravity, fineness modulus, and water absorption values of 2.62, 2.28, and 1.65, respectively. The chemical oxide composition percentages of FA and SS are detailed in Table 1. To create the fly ash-based geopolymer, an alkaline activator solution (AAS) was developed using high-purity laboratory-grade NaOH at 96% purity and Na_2SiO_3 at 97% purity, obtained from Central Drug House (P) Ltd. Three different molarities (M) of NaOH, namely 6M, 12.5M, and 16M, with a NaOH to Na_2SiO_3 ratio of 1, were considered to produce the fly ash-based geopolymer coating. In the end, this coating was integrated into a 12.5M NaOH AAS to develop a geopolymer binder based on fly ash, intended for use in concrete production.

2.2 Mix Design Proportion

The specific combination of mix percentages employed in the study is outlined in Table 2. The weight ratio of Na_2SiO_3 to NaOH, set at 1, aligns with the recommended range of (0.25 - 2.5) for fly ash geopolymer concrete, aiming to enhance compressive strength[33]. A manual mixing process lasting 10

Table 1 — Percentage oxide composition (wt. %).

Chemical composition	SiO_2	Al_2O_3	Fe_2O_3	TiO_2	CaO	K_2O	MgO	MnO	P_2O_5	Na_2O	SO_3
Fly Ash (FA)	55.20	28.80	4.75	1.67	1.21	1.14	0.72	-	0.31	0.24	0.20
Steel Slag (SS)	20.30	5.58	17.70	0.66	43.1	-	7.40	1.74	1.53	0.22	0.26

Table 2 — Mix proportion of fly ash geopolymer coated BOF steel slag concrete (kg/m^3).

Sample ID	Fly Ash	Fine Aggregate (River Sand)	Coarse aggregate (Steel slag)	AAS to FA ratio
6SSGC	445	742	1280	0.45
12.5SSGC	445	742	1280	0.45
16SSGC	445	742	1280	0.45

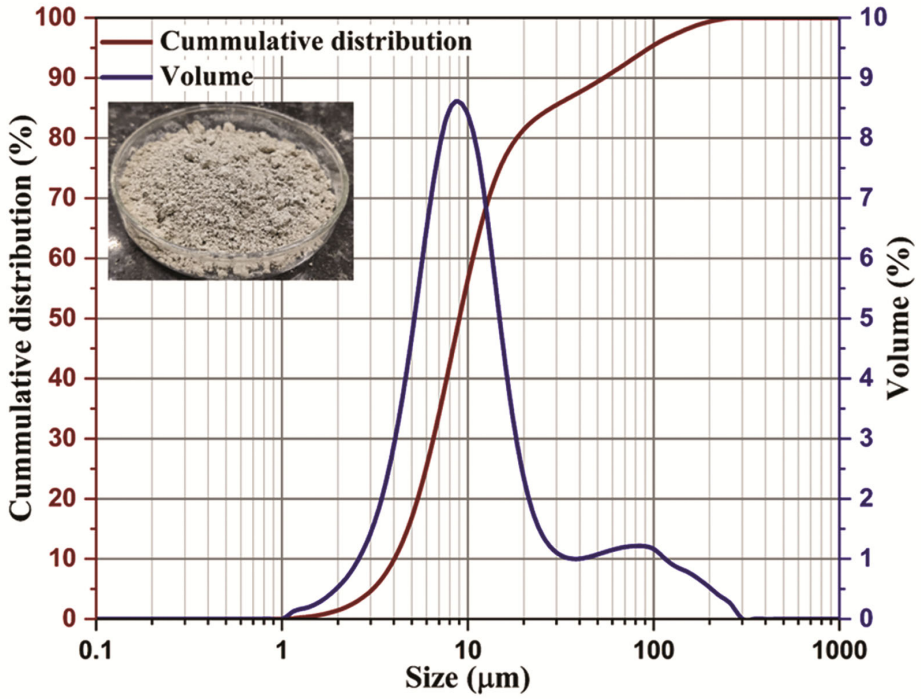

Fig. 1 — Fly ash cumulative and volumetric distribution.

minutes was applied to achieve a homogeneous blend of FA, RS, and SS in varying proportions (prepared according to the process depicted in Fig. 1). Subsequently, 12.5M AAS was incorporated based on the specific mix proportions outlined in Table 2. The mixture underwent an additional 10-minute mixing period at room temperature before being moulded in three layers into cube moulds dimensioning 150 x 150 x 150 mm³, with each layer subjected to 25 times rod tamping for compressive strength test[34]. Electric vibrating tables were employed to compact the specimens for 30 seconds. Following compaction, after 48 hours of curing at 60°C, all specimens were stored at ambient temperature until the compressive strength testing days.The compressive test of cubes was evaluated at 7 and 28 days, following to the guidelines specified in IS 516:1959 (Reaffirmed 2018)[34].

2.3 Characterisation of Material

Particle Size Distribution was analysed using the LA-950V2 Scattering Particle Size Distribution Analyzer, as depicted in Fig. 2. Rigaku X-ray diffractometer was employed for intensity measurements via XRD, covering an angular range of 20-80° and recording Bragg's 2θ. To ascertain the specific functional groups, present in the selected raw materials, FT-IR analysis within the wavenumber range of 400 to 1800 cm^{-1} was conducted using a Bruker spectrometer. SEM micrographs of the materials were generated using a Jeol microscope. The microstructure analysis of the developed concrete was observed using a LEICA DM 2700M optical microscope.

3 Results and Discussion

The study utilized various techniques, including XRF, SEM, XRD, FT-IR, and Optical microscopy, to analyse and characterize materials like FA and SS. These analyses aimed to offer a sound understanding of the materials and validate the effectiveness of geopolymer-coated BOF steel slag when employed as aggregate in a sequence of axial compressive strength tests. The ensuing sections provide interpretations of the results and discussions on these findings.

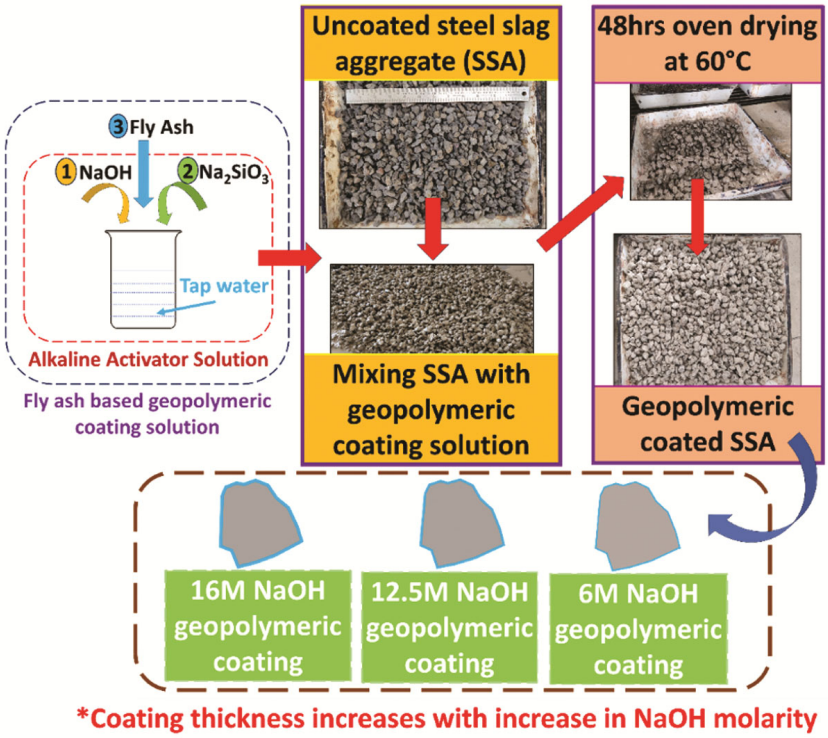

Fig. 2 — Illustration depicting the process of fly ash geopolymer coated steel slag aggregate production.

3.1 Microstructural analysis

3.1.1 X-ray fluorescence (XRF) analysis

he chemicaloxide composition of FA and SS was investigated using XRF, the outcomes are presented in Table 1. In fly ash (FA), the predominant oxide compositions are SiO_2 (55.20%), Al_2O_3 (28.80%), and Fe_2O_3 (4.75%), while SS is characterized by CaO (43.1%), SiO_2 (20.30%), and Fe_2O_3 (17.70%). The XRF values of fly ash, as per IS 3812, categorize it as class-F [30, 34]. Notably, SS exhibits a calcium oxide content of 43.10%, contributing to its expansion properties, and an iron oxide content of 17.70%, which enhances the density of the aggregate and, consequently, the concrete.

3.1.2 Particle size analysis of fly ash (FA)

A fundamental aspect of evaluating any raw material or by product is its particle size. The particle size distribution and sieve analysis are depicted in Fig. 1, illustrating a range from 1 to 300 µm. The distribution reveals significant volume reductions in the 7 – 9 µm range, with an effective particle size of D_{10} = 4.085 µm and D_{90} = 71.923 µm.

3.1.3 Morphology (SEM) analysis

The scanning electron microscopy examination was investigated to evaluate the shape and size, angular characteristics, and surface texture of both FA and SS raw particles, as illustrated in Fig. 3. The examination revealed that FA exhibited a spherical shape, with the maximum particle size being approximately 10 µm, a characteristic further supported by the particle size distribution curve in Fig. 4(a). Additionally, Fig. 4(b) displays various particle sizes and shapes of SS. It can be asserted that the diverse angular shapes of SS particles offer a larger surface area, providing more sites for physical bonding within the matrix, a characteristic also validated by the observed compressive strength.

3.1.4 XRD analysis

Figure 4 depicts the diffraction peak analysis of FA, which validates the presence of prominent peaks of silicon dioxide (SiO_2), i.e., quartz at 2θ = 26.6°, iron oxide (Fe_2O_3) i.e., haematite at 2θ = 35.2°, magnetite peaks at 2θ = 30.9° and 50°, and the aluminium silicate (Al_2O_3. SiO_2) at 2θ = 33.2° and 40.8°[35, 36]. The presence of elements in the XRD minerals phases of FA is also confirmed by the XRF oxide composition tabulated in Table 1, which confirms the presence of oxides that are required in class-F fly ash and essential for geopolymerization. Whereas the complex crystalline phases of SS confirm the presence of primary main peaks of

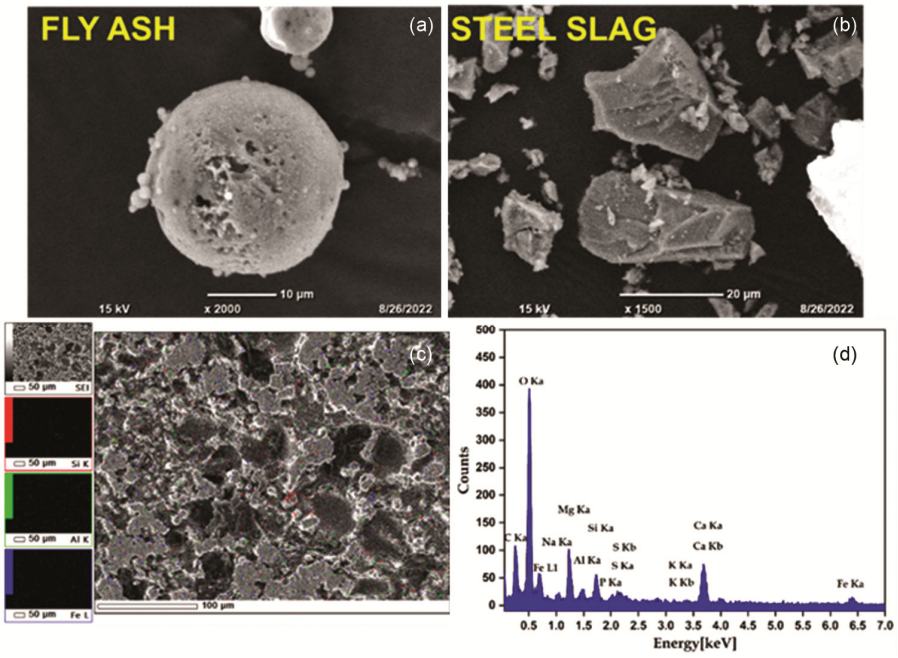

Fig. 3 — (a) Morphology of fly ash, (b) Morphology of BOF steel slag, (c) SEM image of geopolymer concrete, and (d) SEM-EDS elemental analysis of geopolymer concrete.

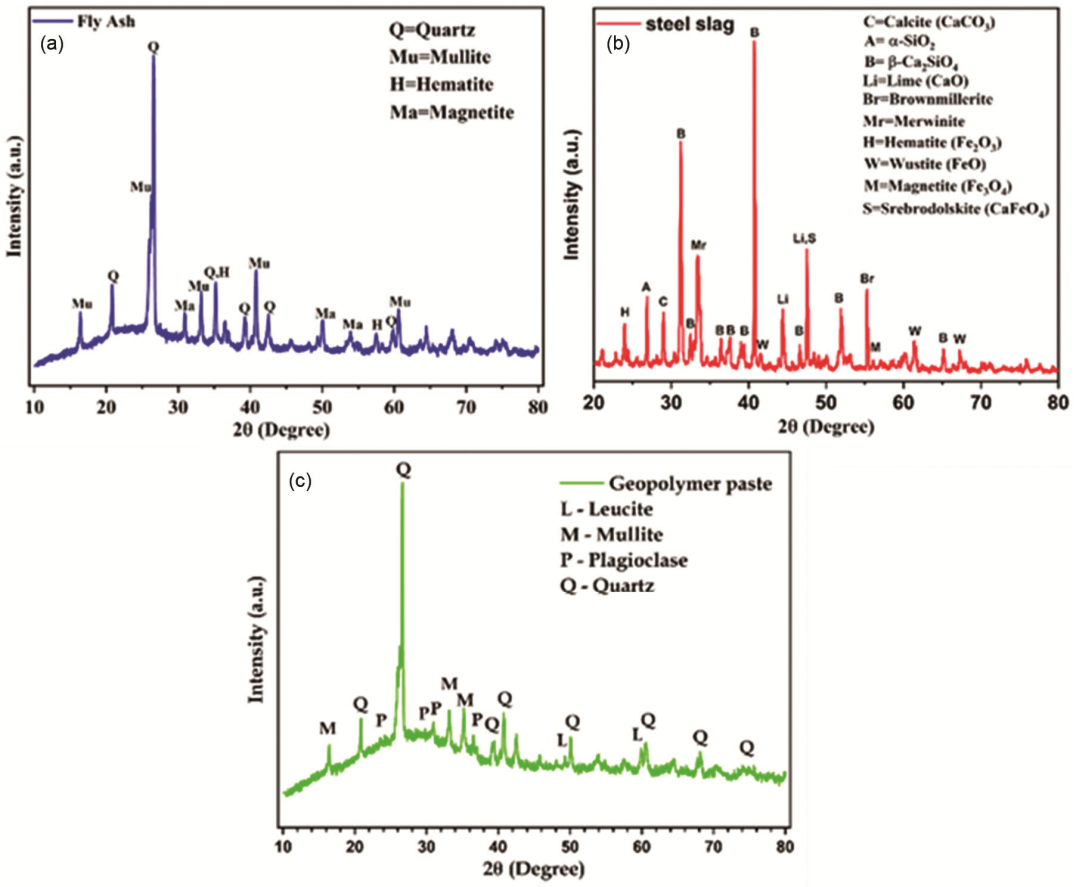

Fig. 4 — (a) XRD analysis of fly ash, (b) XRD analysis of BOF steel slag, and (c) XRD analysis of geopolymer paste.

(β)-calcium silicate ($2CaO.SiO_2$) at 2θ = 31.2° and 40.7°, lime (CaO) at 2θ = 47.5°, merwinite at 2θ = 33.4°, brownmillerite at 2θ = 55.3° and (α) silicon dioxide at 2θ = 26.9°[36-38]. Mineralogical investigation of SS revealed phases responsible for the cementitious material property, which is deduced in the enhancement of compatibility with geopolymerbinder and improved performance of concrete[39].Peaks at 2θ = 49.5° and 59.8° confirm the presence of leucite ($KAlSi_2O_6$), while peaks at 2θ = 23.8°, 29.9°, and 30.2° indicate the presence of plagioclase ($NaAlSi_3O_8$-$CaAl_2SiO_8$). The broad hump in geopolymer paste between 2θ = 25-35° corresponds to the geopolymerization level[40].

3.1.5 FT-IR analysis

Figure 5 shows the FT-IR analysis investigated on both SS and FA. The spectral band detected at 1739 cm^{-1} corresponds to the stretching vibration of C-H bonds in both materials, indicating the existence of residual hydrocarbons. Additionally, the peak at 1470 cm^{-1} matches O-C-O bending vibration, attributed to the carbonate position in SS. In FA, the region at 1367 cm^{-1} is associated with the presence of CaO, a finding corroborated by XRF and XRD data. The finger region at 1057 cm^{-1} in FA suggests Si-O-Si stretching vibration of SiO_2, a result supported by XRF and XRD data. The range between 975 to 925 cm^{-1} in SS confirms Si-O stretching vibration, indicative of the presence of quartz, a fact supported by XRF data. At 850 cm^{-1} in SS, O-C-O asymmetric vibration is noted, attributed to the calcite content, which was also found in the XRD phase. The finger region at 792 cm^{-1} in FA relates to Si-O-T (T = Si or Al) symmetric vibration, while the range between 500 to 430 cm^{-1} in SS signifies the iron oxide group, and the range between 550 to 430 cm^{-1} confirms the presence of Si-O-T (T = Si or Al) of the hematite group. Fig. 5 depicts the FT-IR analysis of geopolymer paste. The presence of carbonate, indicated by the C-O stretching vibration at 1456 cm^{-1} in the finger region, confirms carbonization. The spectral band observed at 1007 cm^{-1} is indicative of the asymmetric vibration of Si-O-Si bonds, suggesting the formation of N-A-S-H gel and/or C-A-S-H gel during the geopolymerization process[41, 42]. Moreover, the presence of a peak at 776 cm^{-1} signifies the symmetric vibration of Si-O-T (where T = Si or Al), whereas the peak at 691 cm^{-1} corresponds to the bending vibration of Si-O-Si in quartz (SiO_2). Additionally, the spectral range between 575 to 450 cm^{-1} confirms the stretching vibration of Si-O-T (where T = Si or Al)[43].

3.2 Compressive strength

Figure 6 illustrates the changes in the compressive strength capacity with varying molarities of geopolymer coating. The compressive strength of 6SSGC is the least among the three samples, measuring 15 MPa and 22 MPa at 7 and 28 days, respectively. In contrast, the 16SSGC sample exhibits the highest compressive strength at both time points, recording 22 MPa and 32 MPa at 7 and 28 days, respectively. This translates to a 46.67% and 22.22% higher compressive strength at 7 days compared to the 6SSGC and 12.5SSGC samples, respectively. Similarly, at 28 days, the 16SSGC sample demonstrates a 45.45% and 23.07% higher compressive strength than the 6SSGC and 12.5SSGC samples, respectively. The results indicate a direct

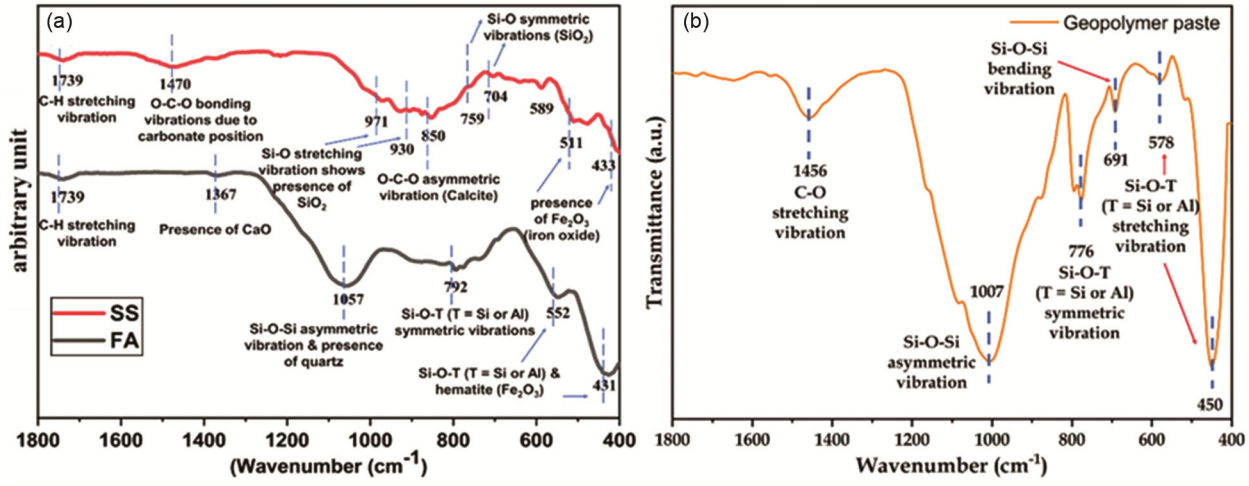

Fig. 5 — (a) FT-IR analysis of BOF steel slag and fly ash, and (b) FT-IR analysis of geopolymer paste.

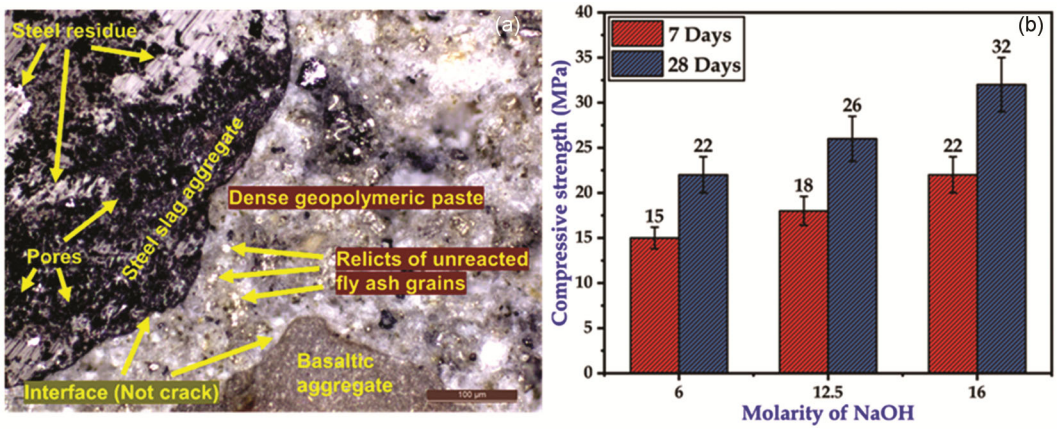

Fig. 6 — (a) Geopolymer concrete microstructure analysis using an optical microscope, and (b) Comparative compressive strength versus Molarity plot.

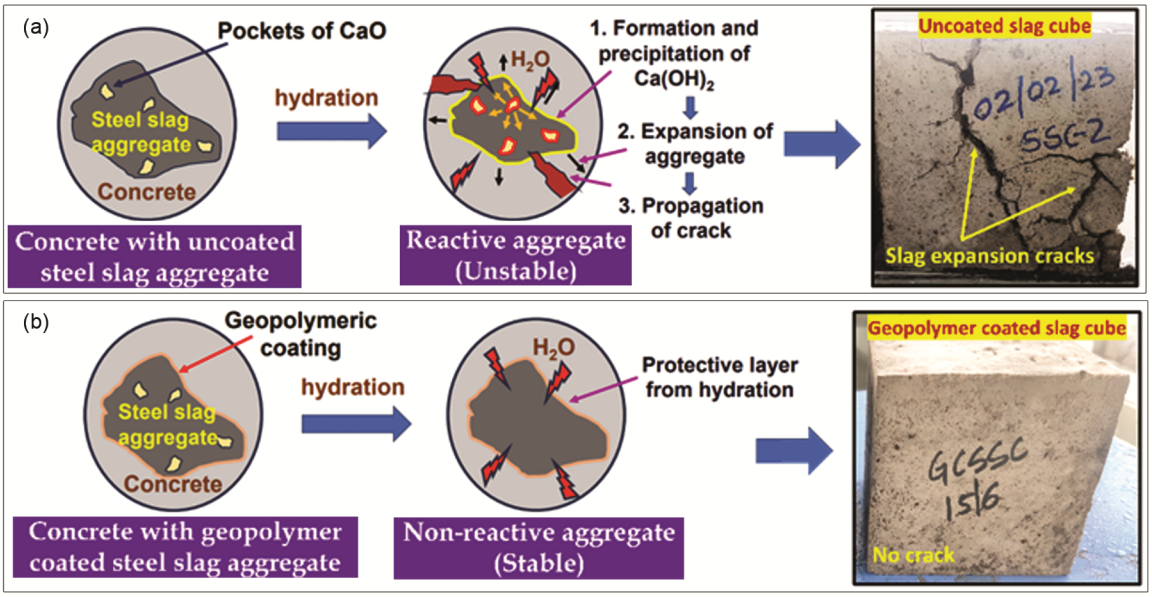

Fig. 7 — (a) Steel slag expansion mechanism, and (b) Steel slag expansion mitigation mechanism.

correlation between molarity and geopolymerization, highlighting enhanced binding properties between the geopolymer matrix and SS coarse aggregate, showing improved compressive strength. Fig. 6 visually captures the dense microstructure of geopolymer concrete, showcasing the superior performance of geopolymer-coated BOF steel slag as aggregate within geopolymer concrete. Additionally, Fig. 7 illustrates the mechanism of crack mitigation, revealing a stable concrete volume without any cracks. This observation confirms the feasibility of utilizing geopolymer-coated BOF steel slag aggregate in geopolymer concrete.

4 Conclusion

The current study explored the mechanism for mitigating expansion in BOF SS by employing three distinct sodium hydroxide (NaOH) molarities in an alkaline activator solution. The study also assessed the potential of employing treated BOF SS as a substitute of natural coarse aggregate in fly ash geopolymer concrete. An elevated molarities of sodium hydroxide in the alkaline activator solution leads to a denser geopolymer paste, which effectively restrains f-CaO hydration and enhances volumetric stability in both the BOF SS aggregate and the resulting concrete matrix. With the rise in sodium

hydroxide molarity within the alkaline activator solution, geopolymerization amplifies, facilitating enhanced bonding between the aggregate and geopolymeric paste, resulting in enhanced mechanical characteristics. At 28 days, concrete containing geopolymer-coated BOF steel slag aggregate with a sodium hydroxide molarity of 16 exhibited the maximum compressive strength of 32 MPa, while concrete with a sodium hydroxide molarity of 6 showed the lowest compressive strength of 22 MPa. In summary, the geopolymer coating mechanism eliminates the need for aging or weathering of BOF steel slag. This experimental research demonstrates the effective utilization of geopolymer-coated BOF SS as coarse aggregate in a fly ash geopolymer binder medium for unreinforced concrete products. This method aids in minimizing and managing waste, improving the handling of materials, and preventing soil contamination and pollution.

Acknowledgement

The authors extend sincere gratitude to the Directors of CSIR-AMPRI, Bhopal, and UTD-CSVTU, Bhilai, for their invaluable scientific and technical guidance. Appreciation is also extended to AICTE, New Delhi, for granting the AICTE Doctoral Fellowship (ADF), as well as to Bhilai Steel Plant (BSP), Bhilai (C.G.), India, and NSPCL, Bhilai, for providing BOF steel slag and Fly Ash, respectively, for the Research & Development.

References

1 El Haggar, S. M., Elsevier, 2005; pp 313-400.
2 Kumar, K.; Bandi, J.; Tenneti, L. The Indian steel industry: Growth, challenges and digital disruption. PwC India 2019, 27.
3 World Steel in Figures Report, 2021 Brussels.
4 Piro, N. S.; Mohammed, A.; Hamad, S. M.; Kurda, R. Construction and Building Materials 2022, 327, 127008.
5 Reddy, A. S.; Pradhan, R. K.; Chandra, S. International Journal of Mineral Processing 2006, 79 (2), 98-105.
6 Das, B.; Prakash, S.; Reddy, P. S. R.; Misra, V. N. Resour Conserv Recy 2007, 50 (1), 40-57.
7 Tossavainen, M.; Engstrom, F.; Yang, Q.; Menad, N.; Lidstrom Larsson, M.; Bjorkman, B. Waste Manag 2007, 27 (10), 1335-1344.
8 Yi, H.; Xu, G. P.; Cheng, H. G.; Wang, J. S.; Wan, Y. F.; Chen, H. Procedia Environ Sci 2012, 16, 791-801.
9 Singh, S. K.; Rekha, P.; Surya, M. Journal of Material Cycles and Waste Management 2020, 22 (3), 611-627.
10 G.O.I.M.O. Mines, I.B.O. Mines, Indian Minerals Yearbook 2019, Part II, 2019, pp. 1–39.
11 Mudgal, M.; Goyal, P. K.; Ghosh, P. K.; Kumar, A.; Chouhan, R.; Srivastava, A. Australian Journal of Structural Engineering 2024, 1-12.
12 Grönniger, J.; Wistuba, M. P.; Cannone Falchetto, A. In Proceedings of the International Conference on Industrial Wasted and Wastewater Treatment & Valorization, Athens, Greece, 2015; pp 21-23.
13 Chen, S. H.; Lin, D. F.; Luo, H. L.; Lin, Z. Y. Construction and Building Materials 2017, 157, 647-653.
14 Kambole, C.; Paige-Green, P.; Kupolati, W. K.; Ndambuki, J. M.; Adeboje, A. O. Construction and Building Materials 2017, 148, 618-631.
15 Cui, P.; Wu, S.; Xiao, Y.; Liu, Q.; Wang, F. J Hazard Mater 2021, 412, 125344.
16 Fisher, L. V.; Barron, A. R. 146, 244-255.
17 Brand, A. S.; Roesler, J. R. Cement Concrete Comp 2015, 60, 1-9.
18 Yildirim, I. Z.; Prezzi, M. Chemical, mineralogical, and morphological properties of steel slag. Advances in civil engineering 2011, 2011.
19 Palankar, N.; Shankar, A. U. R.; Mithun, B. M. Journal of Cleaner Production 2016, 129, 437-448.
20 Singh, P.; Roy, A. B. D.; Singh, H. Journal of Building Engineering 2022, 61, 105301.
21 Singh, A.; Bhadauria, S. S.; Thakare, A. A.; Kumar, A.; Mudgal, M.; Chaudhary, S. Case Studies in Construction Materials 2024, 20, e02715.
22 Flatt, R. J.; Roussel, N.; Cheeseman, C. R. Journal of the European Ceramic Society 2012, 32 (11), 2787-2798.
23 Gartner, E.; Hirao, H. Cement and Concrete Research 2015, 78, 126-142.
24 Provis, J. L.; Van Deventer, J. S. Alkali activated materials: state-of-the-art report, RILEM TC 224-AAM; Springer Science & Business Media, 2013.
25 Singh, B.; Ishwarya, G.; Gupta, M.; Bhattacharyya, S. K. Construction and Building Materials 2015, 85, 78-90.
26 Wan-En, O.; Yun-Ming, L.; Cheng-Yong, H.; Li Ngee, H.; Abdullah, M. M. A.; Khalid, M. S. B.; Loong, F. K.; Shee-Ween, O.; Seng, T. P.; Jie, H. Y.; et al. Journal of Cleaner Production 2022, 378, 134370.
27 Bakharev, T. Cement and Concrete Research 2005, 35 (6), 1233-1246.
28 Kong, D. L. Y.; Sanjayan, J. G. Cement Concrete Comp 2008, 30 (10), 986-991.
29 Provis, J. L.; Van Deventer, J. S. J. Geopolymers: structures, processing, properties and industrial applications; Elsevier, 2009.
30 Okoro, W.; Oyebisi, S. Mechanical and durability assessments of steel slag-seashell powder-based geopolymer concrete. Heliyon 2023, 9 (2), e13188. DOI: 10.1016/j.heliyon. 2023.e13188 From NLM PubMed-not-MEDLINE.
31 IS3812. Indian Standard PULVERIZED FUEL ASH — SPECIFICATION PART 2 FOR USE AS ADMIXTURE IN CEMENT MORTAR AND CONCRET (Third Revision). 2013.
32 IS383. Coarse and Fine Aggregate for Concrete Specification. Bureau of Indian Standard: New Delhi, India, 2016. 2016.
33 Imtiaz, L.; Rehman, S. K. U.; Ali Memon, S.; Khizar Khan, M.; Faisal Javed, M. J. A. s. A review of recent developments and

advances in eco-friendly geopolymer concrete. 2020, 10 (21), 7838.

34 IS516. (Reaffirmed 2018) Indian Standard, methods of tests for strength of concrete. 1959.

35 Mudgal, M.; Chouhan, R. K.; Kushwah, S.; Srivastava, A. K. Emerging Materials Research 2019, 9 (1), 2-9.

36 Mudgal, M.; Mishra, A.; Soni, A.; Raghubanshi, A. S.; Kumar, A.; Chouhan, R. K.; Singh, A.; Srivastava, A. K. Silicon 2022, 14 (17), 11293-11302.

37 Shen, H. T.; Forssberg, E.; Nordström, U. Resour Conserv Recy 2004, 40 (3), 245-271.

38 Tsakiridis, P. E.; Papadimitriou, G. D.; Tsivilis, S.; Koroneos, C. J Hazard Mater 2008, 152 (2), 805-811.

39 Mo, L. W.; Zhang, F.; Deng, M.; Jin, F.; Al-Tabbaa, A.; Wang, A. G. Cement Concrete Comp 2017, 83, 138-145.

40 Phoo-ngernkham, T.; Chindaprasirt, P.; Sata, V.; Hanjitsuwan, S.; Hatanaka, S. Materials & Design 2014, 55, 58-65.

41 Wang, H.; Zhao, X.; Zhou, B.; Lin, Y.; Gao, H. Materials 2020, 13 (24), 5604.

42 Moreno-Maroto, J. M.; Delgado-Plana, P.; Cabezas-Rodríguez, R.; de Gutiérrez, R. M.; Eliche-Quesada, D.; Pérez-Villarejo, L.; Galán-Arboledas, R. J.; Bueno, S. Journal of Cleaner Production 2022, 330, 129770.

43 Ma, G.; Yan, Y.; Zhang, M.; Sanjayan, J. Ceramics International 2022, 48 (18), 26233-26247.